Griffiths, D. V. & Marquez, R. M. (2007). *Géotechnique* **57**, No. 6, 537–546 **doi:** 10.1680/geot.2007.57.6.537

Three-dimensional slope stability analysis by elasto-plastic finite elements

D. V. GRIFFITHS* and R. M. MARQUEZ*

Slope stability analysis is one of the oldest applications in geotechnical engineering, yet it remains one of the most active areas of study in both research and practice. The vast majority of slope stability analyses are performed in two dimensions under the assumption of plane strain conditions. Even when two-dimensional (2D) conditions are not appropriate, three-dimensional (3D) analysis is rarely performed. There are a number of reasons for this. The majority of work on this subject strongly suggests that the 2D factor of safety is conservative (i.e. lower than the 'true' 3D factor of safety). Even when 3D may be justified on geometric grounds, the available methods, being often based on extrapolations of 2D 'methods of slices' to 3D 'methods of columns', are complex, involve numerous assumptions, and are not readily modified to account for realistic boundary conditions in the third dimension such as sloping abutments. The power and versatility of the elasto-plastic finite element approach to slope stability analysis in 2D are well known, and these advantages are even more attractive in 3D. The paper demonstrates some 3D slope stability analyses by finite elements, placing the results in context with 2D solutions and validating the results where possible against alternative methods.

KEYWORDS: failure; limit equilibrium methods; numerical modelling; plasticity; pore pressures; slopes

L'analyse de la stabilité des versants représente l'une des plus anciennes applications en ingénierie géotechnique. Elle reste pourtant l'une des disciplines d'étude les plus actives, en recherche et en pratique. La grande majorité des analyses de stabilité des versants est réalisée en deux dimensions, en considérant des conditions de déformation plane. Même lorsque des conditions à deux dimensions ne sont pas adaptées, il est rare que des analyses à trois dimensions soient effectuées, et ce pour un certain nombre de raisons. La majorité des travaux à ce sujet suggère fortement que le coefficient de sécurité 2D est conservateur (c'est-à-dire inférieur au « vrai » coefficient de sécurité 3D). Même lorsque des raisons géométriques justifieraient la 3D, les méthodes disponibles, souvent basées sur des extrapolations de « Méthode de coupes » 2D en « Méthode de colonnes » 3D, sont complexes, s'appuient sur de nombreuses hypothèses et ne peuvent être aisément modifiées pour tenir compte de conditions de frontière réalistes en 3D, telles que des culées inclinées. La puissance et la versatilité de l'approche des éléments finis en comportement élasto-plastique pour l'analyse de la stabilité des versants en 2D sont bien connues, et ces avantages sont encore plus prometteurs en 3D. Cet article présente certaines analyses de stabilité de versants en 3D en adoptant la méthode des éléments finis, mettant les résultats en contexte avec les solutions 2D et les validant contre des méthodes alternatives lorsqu'il est possible.

INTRODUCTION

Slope stability analysis remains an active and important area of study for geotechnical engineers, both in practice and in academia. The vast majority of slope stability analysis is performed in two dimensions, without much consideration being given to the appropriateness of that assumption, or the impact that a more realistic three-dimensional (3D) analysis would have.

There are a number of reasons for this apparent omission. Most importantly, the two-dimensional (2D) factor of safety is generally considered to be conservative (i.e. lower than the 'true' 3D factor of safety), so practitioners are reluctant to invest in the more time-consuming 3D approaches. A further disadvantage of some 3D methods is that, being based on extrapolations of 2D 'methods of slices' to 3D 'methods of columns' (e.g. Stark & Eid, 1998, Chen *et al.*, 2005), they contain many assumptions relating to side forces that are not easily justified, and the methods are not readily modified to account for realistic geometries and boundary conditions in the third dimension such as sloping abutments. Furthermore, in cases where the critical failure surface is initially unknown, it is difficult to set up general algorithms that would search for the critical failure surface, especially in cases where it may not be spherical.

The assumption that 2D analyses lead to conservative factors of safety needs some qualification, however. First, a conservative result will be obtained only if the most pessimistic section in the 3D problem is selected for 2D analysis (e.g. Duncan, 1996a). In a slope that contains layering and strength variability in the third dimension, this 'most pessimistic' section may not be intuitively obvious. Second, as pointed out by Arellano & Stark (2000), the corollary of a conservative 2D slope stability analysis is that back-analysis of a failed slope will lead to an *unconservative* overestimation of the soil shear strength. Although Hutchinson & Sarma (1985) and Hungr (1987) have both asserted that the factor of safety in 3D is always greater than in 2D, it cannot be ruled out that an unusual combination of soil properties and geometry could lead to a 3D mechanism that is more critical. Bromhead (2004) argued that some landslide configurations with highly variable cross-sections could lead to failure modes in which the 3D mechanism was the most critical. Other investigators have indicated more critical 3D factors of safety (e.g. Chen & Chameau, 1982; Seed *et al.*, 1990), although this remains a controversial topic (see Table 1 later for a summary of recent papers).

The potential benefits of the elasto-plastic finite element (FE) approach to slope stability analysis in 2D are well

Manuscript received 8 February 2006; revised manuscript accepted 5 March 2007.
Discussion on this paper closes on 1 February 2008, for further details see p. ii.
* Division of Engineering, Colorado School of Mines, Golden, USA.

Table 1. 3D slope stability methods

Authors	Method
Chen *et al.* (2001)	Upper-bound plasticity
Huang *et al.* (2002)	Limit equilibrium
Chang (2002)	Limit equilibrium
Chugh (2003)	Finite differences
J. Chen *et al.* (2003)	Limit equilibrium
Z. Chen *et al.* (2003)	Upper-bound rigid FE
Farzaneh & Askari (2003)	Upper-bound analysis
Xie *et al.* (2003)	Limit equilibrium
Bromhead & Martin (2004)	Limit equilibrium
Sainak (2004)	Finite elements
Loehr *et al.* (2004)	Limit equilibrium
Jiang & Yamagami (2004)	Spencer's method
Chen *et al.* (2005)	Upper-bound rigid FE
Zhang *et al.* (2005a, 2005b)	Extended Janbu
Chang (2005)	Sliding blocks
Silvestri (2006)	Analytical
Xie *et al.* (2006)	GIS methods

known, and were summarised by Griffiths & Lane (1999) as follows:

(*a*) No assumption needs to be made in advance about the shape or location of the failure surface. Failure occurs 'naturally' through the zones within the soil mass in which the soil shear strength is unable to sustain the gravitationally generated shear stresses.
(*b*) Since there is no concept of slices or columns in the FE approach, there is no need for assumptions about side forces and the consequent implications for local and global equilibrium. The finite element method preserves global equilibrium until 'failure' is reached.
(*c*) If realistic soil compressibility data are available, the FE solutions will give information about deformations at working stress levels.
(*d*) The FE method is able to monitor progressive failure up to and including overall shear failure in, for example, an analysis involving sequential construction of an excavation or embankment.

Thanks to the remarkable increase in computational power and falling costs in recent years, meaningful 3D analysis can now be performed on a conventional desktop or laptop computer. A free 3D FE slope stability analysis program is described in detail in the text by Smith & Griffiths (2004), and can be downloaded from the web.†

While 2D and 3D slope stability analyses are not expected to give significantly different results in many cases, the availability of accurate and inexpensive software for 3D analysis makes the use of 2D approaches for all cases harder to defend. Perhaps the best justification for promoting 3D analysis at this stage lies mainly in advancing the state of the art. Three-dimensional analysis is more realistic in being able to account properly for the fixity and geometry of abutments in the third dimension. This leads not only to improved accuracy, but also to a better understanding of the fundamental nature of slope failure mechanisms.

RECENT ACTIVITY

It is fair to say that, at the time of writing, 3D slope stability analysis is performed so rarely in practice that there is no 'standard' method (analogous to Bishop's method, say) that is widely accepted by geotechnical engineers. There has been significant activity in recent years on 3D analysis techniques, however, with many of the methods based on extrapolations of 2D analyses. Using a similar format to Duncan (1996b), Table 1 provides a list of 3D slope stability publications that have appeared in the last five years. Although direct comparisons with 2D results were not directly presented in all these papers, the overwhelming majority either stated or implied that 3D analysis gave higher factors of safety than 2D analysis, provided the most critical cross-section was selected for the 2D analysis.

† www.mines.edu/∼vgriffit/4th_ed/Software

BRIEF REVIEW OF FINITE ELEMENTS IN SLOPE STABILITY

The elasto-plastic FE method has been shown to be a powerful alternative to conventional slope stability analysis techniques (e.g. Smith & Hobbs, 1974; Zienkiewicz *et al.*, 1975; Griffiths, 1980). The first published FE slope stability software was reported in the second edition of the text by Smith & Griffiths (1988), and increased use of the method by other researchers over the years (e.g. Kidger, 1990; Potts *et al.*, 1990; Matsui & San, 1992; Jeremic, 2000; Sainak, 2004) has now led to its inclusion in several proprietary geotechnical software packages.

The FE program used in the present paper employs a 3D analysis of elastic-perfectly plastic soils with a Mohr–Coulomb failure criterion assuming zero dilation. Although any 3D FE could be used in principle, the current work utilises 20-node hexahedral elements with 'reduced integration' (eight Gauss points per element: see e.g. Zienkiewicz, 1977; Hughes, 1987) in the stiffness matrix generation and stress redistribution phases of the algorithm. This element was chosen because it is the 3D counterpart of the 8-node plane element used successfully by the authors and other investigators in the past to model 2D collapse problems.

It is well documented that the factor of safety of slopes assuming elastic-perfectly plastic constitutive models is insensitive to the construction sequence (e.g. Smith & Griffiths, 2004). In the current study, therefore, stresses are applied to an initially weightless FE mesh through the generation of gravity loads that are applied in a single increment. The stresses developed from the addition of gravity are then compared with the Mohr–Coulomb failure criterion. If the resulting stresses at a particular Gauss point lie within the Mohr–Coulomb failure envelope then that point is assumed to remain elastic. Alternatively, if the stresses lie outside the failure envelope, yielding of that point has occurred, and the non-linear parts of the algorithm are activated. The resulting stresses in the yielding regions are redistributed to neighbouring elements that still have reserves of strength, using a viscoplastic algorithm (e.g. Perzyna, 1966; Zienkiewicz & Cormeau, 1974). The algorithm is iterative, since redistribution of stresses in one yielding region may initiate yielding in neighbouring regions that were initially elastic. This iterative process continues until the formation of a failure mechanism consisting of a contiguous zone of soil at failure.

Properties of soil model

To model the soil mass during the FE analysis, the program utilises the six parameters shown in Table 2. The key parameters are the total unit weight γ and the shear strength parameters ϕ' and c' (or $\phi_u = 0$ and c_u in undrained analysis). For the examples presented in this paper, the elastic parameters Young's modulus and Poisson's ratio were assigned nominal values of 10^5 kN/m^2 and 0·3 respectively, for both drained and undrained analyses, as they have

Table 2. Six-parameter soil model

ϕ' (ϕ_u)	Friction angle
c' (c_u)	Cohesion
ψ	Dilation angle
E' (E_u)	Young's modulus
ν' (ν_u)	Poisson's ratio
γ	Unit weight

little influence on the computed factor of safety (e.g. Hammah *et al.*, 2005).

In this work, the dilation angle ψ was set to zero, implying no volume change during yield. The role of the dilation angle has been discussed in detail elsewhere (e.g. Griffiths & Lane, 1999); however, the practical consideration for all geotechnical limit analysis is that this parameter, which affects volume change during plastic yielding, has relatively little influence on collapse load predictions in unconfined drained problems.

Obtaining a factor of safety

In traditional geotechnical practice the factor of safety is defined as the ratio of the average shear strength of the soil to the average shear stress developed along the critical failure surface. Typically, a factor of safety of about 1·5 is required for design.

Based on the above definition, the current approach is to use a shear strength reduction technique in which factored shear strength parameters c'_f and ϕ'_f, given by

$$c'_f = \frac{c'}{\text{SRF}} \tag{1}$$

$$\phi'_f = \tan^{-1}\left(\frac{\tan\phi'}{\text{SRF}}\right) \tag{2}$$

are used in the analysis, where SRF is a 'strength reduction factor'. In line with conventional slope stability analysis methods, the strength reduction factor is assumed to apply equally to both c' and $\tan\phi'$. In order to obtain the 'true' factor of safety the strength reduction factor is gradually increased until failure of the slope, as described in the next section, occurs. When this critical value has been found, the factor of safety of the slope is equal to the strength reduction factor and FS $\approx$ SRF.

Failure of the slope

In the program used in this study, slope failure is said to have occurred when the algorithm cannot converge within a user-specified iteration ceiling (typically set to 1000). If the algorithm reaches the iteration ceiling it means that the algorithm is unable to find a stress redistribution that will simultaneously satisfy both global equilibrium and the Mohr–Coulomb failure criterion with reduced strength parameters. At this point slope failure occurs, resulting in rapidly increasing nodal displacements in the mesh. Fig. 1 shows a typical graph of SRF against $E'\delta_{max}/\gamma H^2$ (a dimensionless displacement), where δ_{max} is the maximum nodal displacement component at convergence, and H is the slope height.

VALIDATION AGAINST 2D ANALYSIS

An initial step in validating the results was to compare the results from the 3D analyses with those obtained by conventional 2D limit equilibrium analysis. The example geometry shown in Fig. 2(a) is of a homogeneous slope in which the geometry and dimensions in the x–y plane are extended by

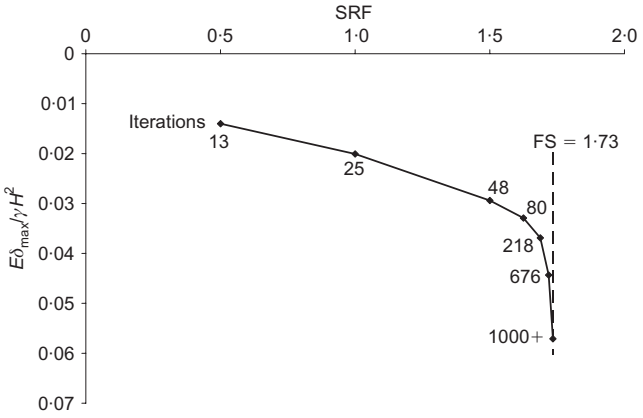

Fig. 1. The rapid increase in the dimensionless displacement along with non-convergence signifies slope failure, at which FS ≈ SRF

a distance $L/2$ (assuming symmetry) in the z direction. Fig. 2(b) shows typical coarser and finer meshes of 20-node elements as used in this study. In both cases, the depth of the mesh in the z direction was altered by simply adding or removing 'slices' of elements in that direction.

The first slope analysed consisted of 'undrained clay' with shear strength given by

$$\phi_u = 0°, \frac{c_u}{\gamma H} = 0{\cdot}20 \tag{3}$$

and elastic properties as indicated above.

The slope is inclined at an angle of 26·57° to the horizontal (2:1 slope), and the boundary conditions are given as 'rough-smooth' for the 3D analysis. Table 3 explains the meaning of the various boundary conditions that can be specified by the user. The 'rough-smooth' boundary condition implies a symmetric analysis about the plane $z = L/2$: thus only half of the actual depth L of the slope is analysed. The bottom ($y = D$) and far side ($z = 0$) of the slope are fully fixed, while the back ($x = 0$) and front side ($z = L/2$) of the slope are constrained by vertical rollers. The dimensions of the slope analysed are given in Table 4. The depth L of the slope is to be varied in the range $H < L < 14H$ (because of symmetry the actual mesh depth varied by half this amount), enabling an investigation to be made of the influence of three-dimensionality. Both the coarser and finer meshes indicated in Fig. 2(b) were run to illustrate the sensitivity of results to mesh refinement.

Table 5 shows results for the specific case of $L = 2H$ (coarser mesh) as SRF was gradually increased. The table shows seven trial strength reduction factors, ranging from 0·5 to 1·734.

The 'Iterations' column displays the number of iterations needed for convergence. As the factor of safety is approached, the algorithm has to work harder to reach convergence, as seen by the increase in the number of iterations. When SRF = 1·73 the analysis was unable to converge within 1000 iterations, and a sudden increase in the dimensionless displacement was observed. At this point FS $\approx$ SRF, and the factor of safety is given by FS $\approx$ 1·73. The results in Table 5 were the actual values plotted in Fig. 1.

Several 3D analyses were performed using both the meshes indicated in Fig. 2(b). In addition, a conventional limit equilibrium analysis was performed on the same cross-section, giving a 2D factor of safety of FS = 1·25. A comparison of the 3D FE and 2D limit equilibrium analyses is given in Fig. 3. The factor of safety in 3D was always higher than in 2D but tended to the plane strain solution for depth ratios of the order of $L/H \approx 10$. It should be noted

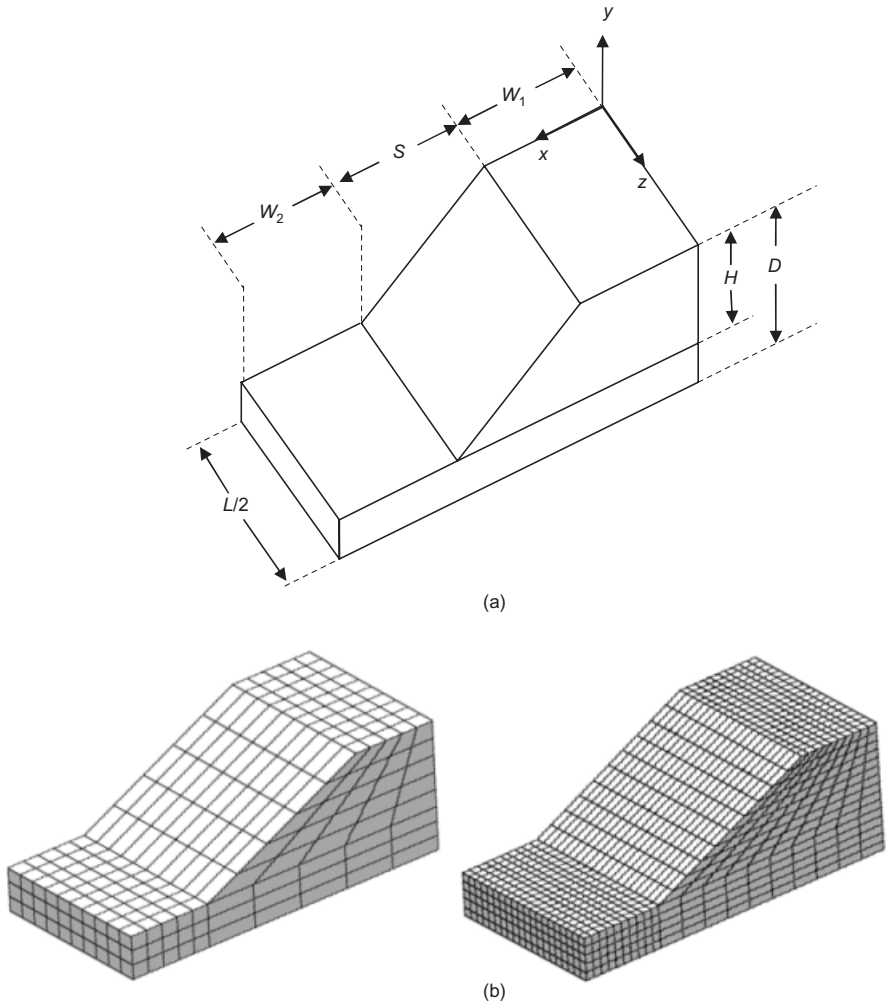

Fig. 2. (a) 3D slope dimensions with uniform section and properties in the z direction; (b) typical coarser and finer 3D meshes of 20-node hexahedral elements (L/H = 2)

Table 3. Description of 3D boundary condition

Plane	Smooth-smooth	Rough-smooth	Rough-rough
$x = 0$	Vertical rollers	Vertical rollers	Vertical rollers
$x = W_1 + S + W_2$	Vertical rollers	Vertical rollers	Vertical rollers
$y = -D$	Fixed	Fixed	Fixed
$z = 0$	Vertical rollers	Fixed	Fixed
$z = L$	Vertical rollers	Vertical rollers ($z = L/2$ for symmetry)	Fixed

Table 4. Dimensions of slope for 2D and 3D analyses

D	W_1	S	W_2	L
1·5H	H	2H	H	$H \rightarrow 14H$

Table 5. 3D results for $L = 2H$ (coarser mesh) with an iteration ceiling of 1000

SRF	$E'\delta_{max}/(\gamma H^2)$	Iterations
0·500	0·701	13
1·000	1·004	25
1·500	1·470	48
1·625	1·645	80
1·6875	1·845	218
1·7188	2·217	676
1·7344	2·855	1000+

that the finer FE mesh always gave slightly lower factors of safety than the coarser mesh, but the difference never exceeded 2%.

OTHER VALIDATION EXAMPLES

For further verification of the present method, a series of 3D analyses is now presented for comparison with results obtained by various investigators using other 3D slope stability techniques. The examples described are typically quite simple, geometrically, and include relatively homogeneous material properties. It should be emphasised that these simplifications are merely to validate the present approach and facilitate comparison with other published results. The

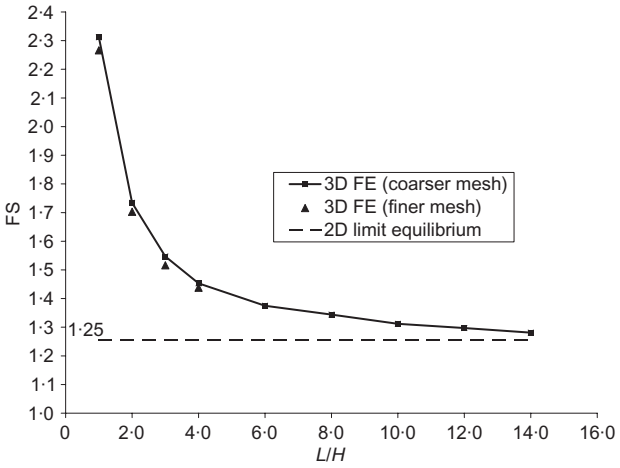

Fig. 3. Comparison of 3D FE and 2D limit analyses for $\phi_u = 0°$ slope with $c_u/\gamma H = 0{\cdot}20$

FE approach described herein requires no such simplifications, since complex geometries and material variability are easily implemented.

Baligh & Azzouz (1975)

In this example a 3D slope was considered as shown in Fig. 4, in which Baligh & Azzouz (1975) suggested a spherical failure surface. From the radius of the sphere, a suitable out-of-plane dimension for the FE mesh was deduced that would force a mechanism in the same general region. In view of the symmetry, 'rough-smooth' boundary conditions were used, as described in Table 3. It should be noted that the spherical failure surface does not necessarily represent the critical failure mechanism: thus in a less confined mesh the FE approach might find a more critical failure path. The results from the FE analysis in the present study, together with results obtained by several other investigators who considered the same slope, are summarised in Table 6. The deformed mesh corresponding to the unconverged solution when SRF = 1·39 is shown in Fig. 5.

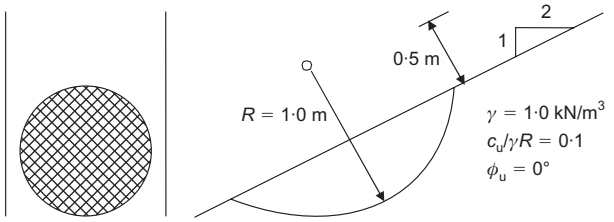

Fig. 4. Plan and section of 3D failure surface in purely cohesive slope as reported by Baligh & Azzouz (1975)

Zhang (1988)

The example shown in Fig. 6 is taken from Zhang (1988) and has been used by various investigators as part of the validation of their particular 3D slope stability methods (e.g. Lam & Fredlund, 1993; Huang & Tsai, 2000; J. Chen *et al.*, 2003). The proposed critical slip surface from limit equilibrium considerations was circular in the x–y plane and ellipsoidal in the out-of-plane direction, which indicated suitable 3D mesh dimensions. Symmetry implied the use once more of 'rough-smooth' boundary conditions.

The problem was analysed for two different cases. In Case 1, the slope is composed of a drained homogeneous soil.

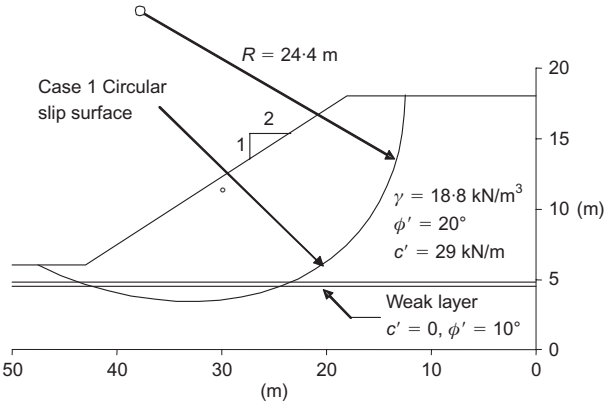

Fig. 6. Cross-section of 3D slope reported by Zhang (1988)

Table 6. Comparison of 3D results (FS) for the slope in Fig. 4

Baligh & Azzouz (1975)	Hungr *et al.* (1989)	Huang & Tsai (2000)	Present study
1·402	1·422	1·399	1·39

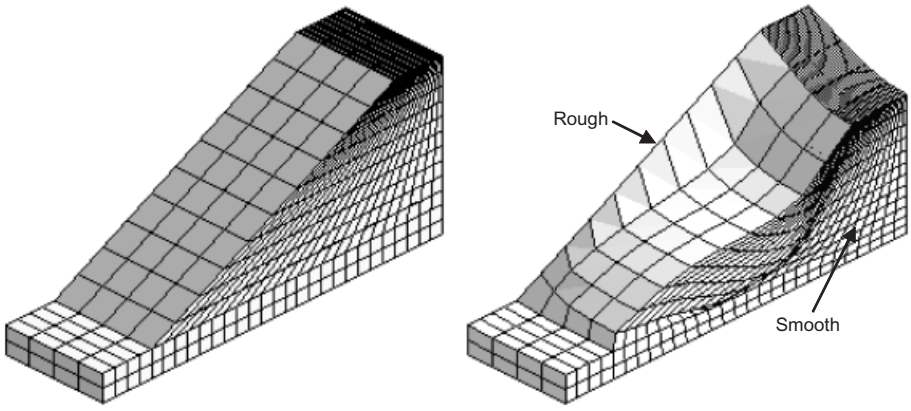

Fig. 5. Undeformed and 'failed' FE meshes for example shown in Fig. 4

The resulting factor of safety of 2·17 from the present study is comparable to those obtained by other investigators, as seen in Table 7. The results found using the package CLARA (Hungr, 1988) were obtained by the authors. Fig. 7 shows the undeformed and 'failed' meshes for this analysis. It can be seen that the failure mechanism is similar to that described in Fig. 6.

Case 2 has the same slope geometry, but includes a weak layer in the foundation of the slope (e.g. geosynthetic layer). Chen *et al.* (2001) used their upper-bound approach to analyse the slope, while a limit equilibrium analysis was used by Chen *et al.* (2003a). The present study yielded a factor of safety of 1·58, which again is in the vicinity of those provided by other investigators, as shown in Table 8. Fig. 8 shows that the failure mechanism concentrated itself along the weak layer, giving a lower factor of safety, as would be expected. Fig. 9 shows the curves of dimensionless displacement against SRF for both cases.

For the relatively simple validation examples shown here, the computed FE results lay well within the quite narrow range of values obtained by other investigators.

The main power of the FE method, however, lies in its ability to deal with more complicated geometries, boundary conditions and property variability. With the confidence gained through the validation examples, the final part of this paper introduces more realistic boundary conditions and examines their influence on the computed factor of safety.

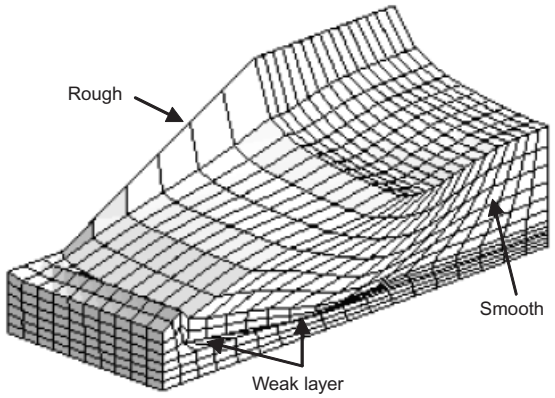

Fig. 8. 'Failed' FE mesh for Case 2 of Zhang (1988) example

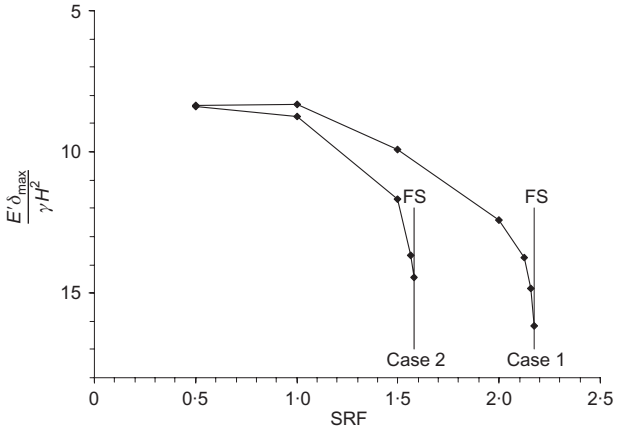

Fig. 9. Dimensionless displacements for Cases 1 and 2 of Zhang (1988) example

INFLUENCE OF SLOPING SIDES

All the examples considered so far had vertical boundaries in the out-of-plane direction. In geotechnical practice it is clearly more likely that these boundaries will be inclined to

Table 7. Comparison of 3D results (FS) from various investigators for Case 1 of Zhang (1988) example

Zhang (1988)	Chen *et al.* (2001)	Chen *et al.* (2003)	CLARA	Present study
2·122	2·262	2·187	2·167	2·17

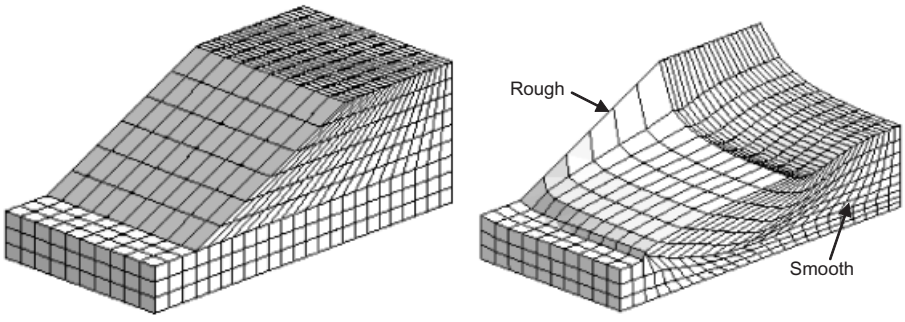

Fig. 7. Undeformed and 'failed' FE meshes for Case 1 of Zhang (1988) example

Table 8. Comparison of 3D results (FS) from various investigators for Case 2 of Zhang (1988) example

Zhang (1988)	Chen *et al.* (2001)	Chen *et al.* (2003)	CLARA	Present study
1·553	1·717	1·603	1·620	1·58

the horizontal, as would be the case at the abutments of an earth dam.

In order to accommodate these changes, a geometry subroutine was developed (Marquez, 2004) to allow the inclination of the side slopes to be controlled through the input data. With this modification, the vertical sides considered earlier can be considered as a special case.

Parametric studies

To help understand the influence of sloping sides a series of tests and comparisons was made. Fig. 10 shows the parameters involved in defining the sloping geometry. In the examples that follow either l_1 or l_2 was held constant while α was varied, with other dimensions fixed to the values given in Table 9. The boundary conditions in this case were 'rough-smooth', with the sloping boundary fully restrained (rough) and the vertical boundary allowed to move freely in the vertical plane (smooth). This analysis implies symmetry, so the actual depth of the embankment modelled was twice the depth of the mesh in the third dimension.

Top depth l_1 held constant

When l_1 is held constant and α is increased, it can be expected that the calculated factor of safety will increase. As α is increased, the soil mass begins to sit more on the abutment or canyon wall. The slope also becomes more confined, resulting in added stability. Two examples were developed, one with $l_1/H = 0{\cdot}833$ and the other with $l_1/H = 1{\cdot}67$. The results for the calculated factor of safety for the two problems can be seen in Fig. 11. It can be seen that the factor of safety for the narrower ($l_1/H = 0{\cdot}833$) slope is greater than that of the deeper slope ($l_1/H = 1{\cdot}67$). The data also show that the influence of α on the slope decreases as the slope becomes wider. This indicates that 3D effects are much more important in narrow slopes than in deep slopes.

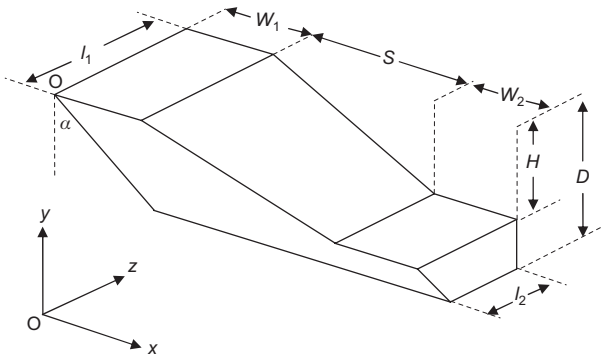

Fig. 10. 3D sloping side geometry

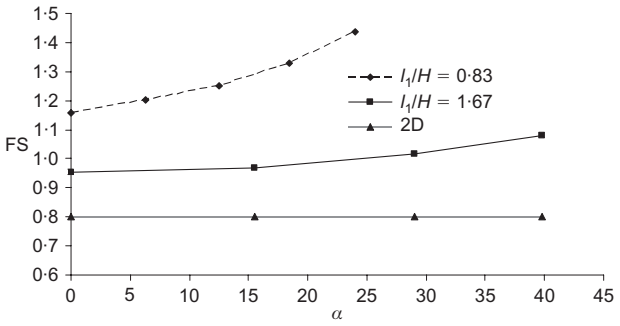

Fig. 11. Results for constant l_1 with $\phi' = 20°$, $c'/\gamma H \approx 0{\cdot}127$ and rough-smooth boundary conditions

Bottom depth l_2 held constant

Another comparison was completed by holding l_2 constant and varying α. This time, as α is increased, it can be expected that the calculated factor of safety will decrease. When l_1 is increased, the soil mass becomes less confined and a failure mechanism can develop more easily. Increasing α in this case results in a less stable slope, with a summary of results shown in Fig. 12.

The 2D result is included in both sets of analyses, emphasising the conservativeness of a 'plane strain' analysis performed at the centreline.

Comparing the results obtained from various trials, it can be seen that the depth of the slope (out-of-plane) and the side slope inclination both have a significant influence on the calculated factor of safety.

INFLUENCE OF VARIABLE STRENGTH

The first example of variable strength involves an undrained clay ($\phi_u = 0°$) with dimensions given in Table 10. The slope is constructed with a 'strong' soil ($c_u/\gamma H = 0{\cdot}263$) near the abutments surrounding a 'weak' soil ($c_u/\gamma H = 0{\cdot}132$) in the central parts of the slope. Sloping sides were included in the analysis with $l_1/l_2 = 2$ and $\alpha = 29°$. Since the slope was no longer symmetrical (the side slope angle on either side differs, as seen in Fig. 13(a)), the boundary conditions used are now 'rough-rough'. The analysis was performed, and the corresponding deformed mesh at failure is shown in Fig. 13(b). The 3D factor of safety was computed as 1·42, while the 2D analysis based on the weaker soil in the centre of the slope gave a factor of safety equal to 0·81.

The second example is similar to that in Fig. 13. The example again assumes undrained soils ($\phi_u = 0$) with dimensions given in Table 11. The strong soil ($c_u/\gamma H = 0{\cdot}263$) is once again surrounding the weaker soil ($c_u/\gamma H = 0{\cdot}132$). The top of the slope l_1 was held constant, with the

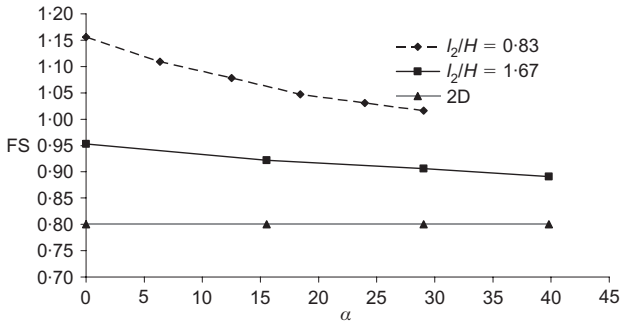

Fig. 12. Results for constant l_2 with $\phi' = 20°$, $c'/\gamma H \approx 0{\cdot}127$ and rough-smooth boundary conditions

Table 9. Dimensions for analyses with sloping sides

D	W_1	S	W_2
$1{\cdot}5H$	H	$2H$	$0{\cdot}66H$

Table 10. Dimensions for the slope in Fig. 13 (see Fig. 10)

D	W_1	S	W_2	l_1	l_2
$1{\cdot}5H$	H	$2H$	$0{\cdot}667H$	$2{\cdot}5H$	$1{\cdot}25H$

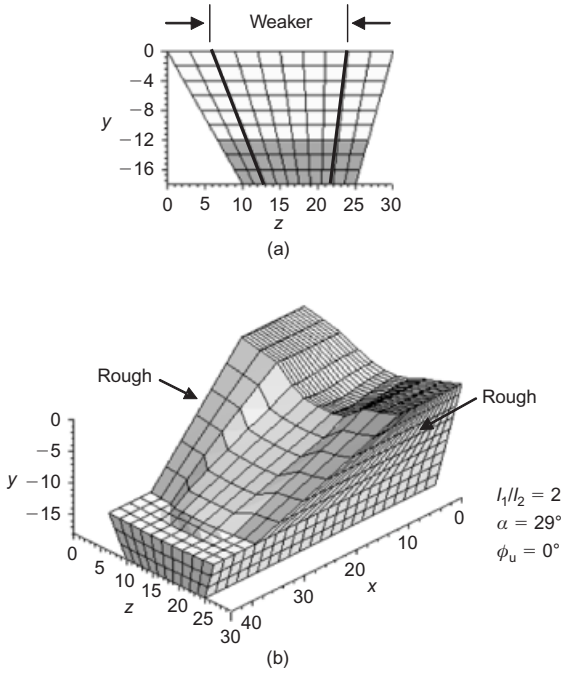

Fig. 13. Finite element mesh displaying a non-symmetric slope with weak soil ($c'/\gamma H$ = 0·132) surrounded by stronger soil ($c'/\gamma H$ = 0·263)

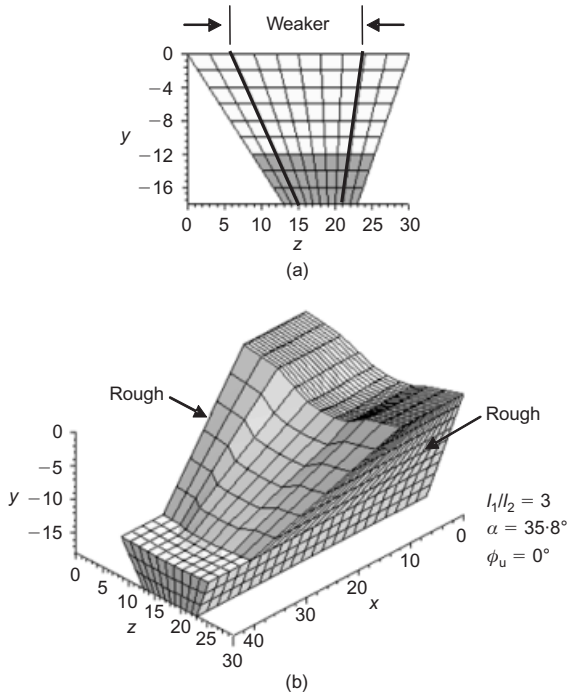

Fig. 14. Finite element mesh showing a more confined slope with weak soil ($c'/\gamma H$ = 0·132) surrounded by stronger soil ($c'/\gamma H$ = 0·263)

Table 11. Dimensions for the slope in Fig. 14

D	W_1	S	W_2	l_1	l_2
1·5H	H	2H	0·667H	2·5H	0·833H

bottom of the slope l_2 decreased to give a ratio of $l_1/l_2 = 3$ and $\alpha = 35·8°$, as shown in Fig. 14(a). The boundary conditions used were again 'rough-rough'. The 3D factor of safety in this case was computed as 1·50, which should be compared with the unchanged 2D factor of safety of 0·81. The deformed mesh at failure is given in Fig. 14(b). A higher 3D factor of safety in this case is to be expected because of the greater confinement of the soil mass provided by the increase in the l_1/l_2 ratio. This is a similar effect to that demonstrated in Fig. 11.

The final example, shown in Fig. 15, utilises symmetry ('rough-smooth' boundary conditions): thus only half the problem is analysed. The slope consists of undrained clay ($\phi_u = 0$) with dimensions given in Table 12. In this case, the strength decreases linearly from $c_u/\gamma H = 0·219$ at the abutments to $c_u/\gamma H = 0·132$ at the centreline. The 3D factor of safety in this case is computed as 1·30, and should be compared with the usual 2D factor of safety of 0·81 at the centreline. The 3D deformed mesh at failure is given in Fig. 15(b). The difference between the 2D and 3D results is still significant but not as pronounced as when there was a step change in strength.

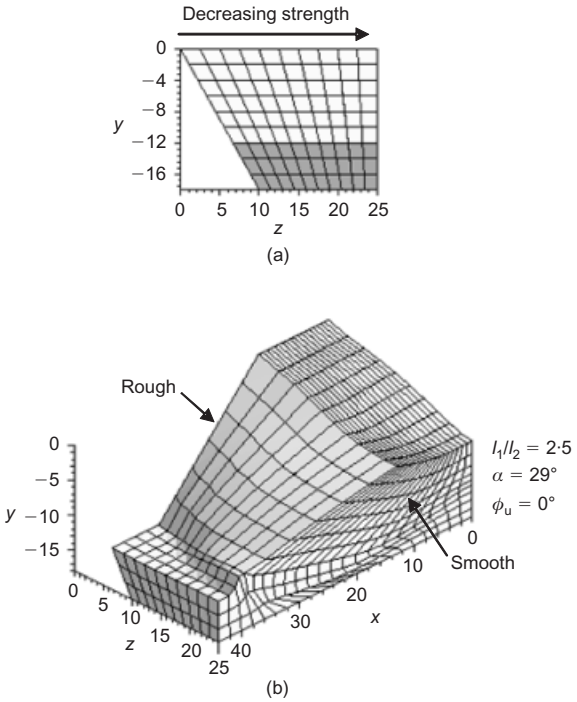

Fig. 15. Finite element mesh with linearly decreasing soil strength

CONCLUDING REMARKS

The FE technique for slope stability analysis has grown significantly in popularity in recent years, owing to its power and versatility. The benefits of the FE approach to 2D slope stability analysis are well documented; however, these advantages over traditional limit equilibrium approaches are even more important in 3D owing to the ease with which

Table 12. Dimensions for the slope in Fig. 15

D	W_1	S	W_2	l_1	l_2
1·5H	H	2H	0·667H	2·08H	1·25H

complex geometries, boundary conditions and property variations in the out-of-plane direction can be introduced. The paper has presented results from several 3D slope examples using an elasto-plastic FE approach. Results were validated against conventional 2D limit equilibrium analyses of a homogeneous slope and demonstrated the convergence of the 3D factor of safety on the 2D result as the out-of-plane dimension was increased. Further examples demonstrated the influence of boundary conditions and confinement in the form of sloping abutments and embankment depth. Finally, some examples were presented that introduced variable strength parameters across the slope in the out-of-plane direction.

While it seems unlikely that 3D slope stability will become a routine approach in geotechnical practice any time soon, the increased speed and falling costs of computers mean that 3D non-linear FE analyses can now be performed routinely on a desktop or laptop computer. Perhaps the best justification for promoting 3D analysis at this stage lies mainly in advancing the state of the art. Three-dimensional analysis is simply more realistic, and leads not only to improved accuracy but also to a better understanding of the nature of slope failure mechanisms.

ACKNOWLEDGEMENT

The authors wish to acknowledge the support of NSF grant CMS-0408150 on 'Advanced probabilistic analysis of stability problems in geotechnical engineering'.

REFERENCES

Arellano, D. & Stark, T. D. (2000). Importance of three-dimensional slope stability analysis in practice. In *Slope Stability 2000*, GSP no. 101 (eds D. V. Griffiths *et al.*), Reston, VA: ASCE, pp. 18–32.

Baligh, M. M. & Azzouz, A. S. (1975). End effects on the stability of cohesive slopes. *J. Geotech. Engng, ASCE* **101**, No. GT11, 1105–1117.

Bromhead, E. N. & Martin, P. L. (2004). Three-dimensional limit equilibrium analysis of the Taren landslide. In *Advances in geotechnical engineering* (Skempton Conference), Vol. 2, pp. 789–802. London: Thomas Telford.

Chang, M. (2002). A 3D slope stability analysis method assuming parallel lines of intersection and differential straining of block contacts. *Can. Geotech. J.* **39**, No. 4, 799–811.

Chang, M. (2005). Three-dimensional stability analysis of the Kettleman Hills landfill slope failure based on observed sliding-block mechanism. *Comput. Geotech.* **32**, No. 8, 587–599.

Chen, J., Yin, J. & Lee, C. F. (2003a). Upper bound limit analysis of slope stability using rigid finite elements and nonlinear programming. *Can. Geotech. J.* **40**, No. 4, 742–752.

Chen, J., Yin, J. H. & Lee, C. F. (2005). A three-dimensional upper-bound approach to slope stability analysis based on RFEM. *Géotechnique* **55**, No. 7, 549–556.

Chen, R. H. & Chameau, J. L. (1982). Three-dimensional limit equilibrium analysis of slopes. *Géotechnique* **32**, No. 1, 31–40.

Chen, Z., Wang, J., Wang, Y., Yin, J. H. & Haberfield, C. (2001). A three-dimensional slope stability analysis method using the upper bound theorem. *Int. J. Rock Mech. Mining Sci.* **38**, No. 3, 379–397.

Chen, Z., Mi, H., Zhang, F. & Wang, X. (2003b). A simplified method for 3D slope stability analysis. *Can. Geotech. J.* **40**, No. 3, 675–683.

Chugh, A. K. (2003). On the boundary conditions in slope stability analysis. *Int. J. Numer. Anal. Methods Geomech.* **27**, No. 11 905–926.

Duncan, J. M. (1996a). Soil slope stability analysis. In *Landslides: Investigation and mitigation*, Special Report 247 (eds A. K. Turner *et al.*), Chapter 13. Washington, DC: Transportation Research Board.

Duncan, J. M. (1996b). State of the art: limit equilibrium and finite-element analysis of slopes. *J. Geotech. Engng* **122**, No. 7, 577–596.

Farzaneh, O. & Askari, F. (2003). Three-dimensional analysis of nonhomogeneous slopes. *J. Geotech. Geoenviron. Engng* **129**, No. 2, 137–145.

Griffiths, D. V. (1980). Finite element analysis of walls, footings and slopes. *Proceedings of the symposium on computer applications to geotechnical problems in highway engineering* (ed. M. F. Randolph), pp.122–146. Cambridge: PM Geotechnical Analysts Ltd.

Griffiths, D. V. & Lane, P. A. (1999). Slope stability analysis by finite elements. *Géotechnique* **49**, No. 3, 387–403.

Hammah, R. E., Yacoub, T. E., Corkum, B. & Curran, J. H. (2005). A comparison of finite element slope stability analysis with conventional limit-equilibrium investigation. *Proc. 58th Canadian Geotechnical and 6th Joint IAH-CNC and CGS Groundwater Specialty Conferences – GeoSask 2005, Saskatoon*, 480–487.

Huang, C. C. & Tsai, C. C. (2000). New method for 3D and asymmetric slope stability analysis. *J. Geotech. Geoenviron. Engng ASCE* **126**, No. 10, 917–927.

Huang, C. C., Tsai, C. C. & Chen, Y. H. (2002). Generalized method for three-dimensional slope stability analysis. *J. Geotech. Geoenviron. Engng, ASCE* **128**, No. 10, 836–848.

Hughes, T. J. R. (1987). *The finite element method*. Englewood Cliffs, NJ: Prentice Hall.

Hungr, O. (1987). An extension of Bishop's simplified method of slope stability analysis to three dimensions. *Géotechnique* **37**, No. 1, 113–117.

Hungr, O. (1988). *CLARA 2·31: Slope stability in two or three dimensions for IBM compatible microcomputers*. Vancouver: O. Hungr Geotechnical Research Inc.

Hungr, O., Salgado, F. M. & Byrne, P. M. (1989). Evaluation of three-dimensional method of slope stability analysis. *Can. Geotech. J.* **26**, No. 4, 679–686.

Hutchinson, J. N. & Sarma, S. K. (1985). Discussion on 'Three-dimensional limit equilibrium analysis of slopes'. *Géotechnique* **35**, No. 2, 215.

Jeremic, B. (2000). Finite element methods for three-dimensional slope stability analysis. In *Slope Stability 2000*, GSP no. 101 (eds D. V. Griffiths *et al.*), Reston, VA: ASCE, pp. 224–238.

Jiang, J. C. & Yamagami, T. (2004). Three-dimensional slope stability analysis using an extended Spencer method. *Soils Found.* **44**, No. 4, 127–135.

Kidger, D. J. (1990). *Visualisation of finite element eigenvalues and three-dimensional plasticity.* PhD thesis, Department of Engineering, University of Manchester.

Lam, L. & Fredlund, D. G. (1993). A general limit equilibrium model for three-dimensional slope stability analysis. *Can. Geotech. J.* **30**, No. 6, 905–919.

Loehr, J. E., McCoy, B. F. & Wright, S. G. (2004). Quasi-three-dimensional slope stability analysis method for general sliding bodies. *J. Geotech. Geoenviron. Engng, ASCE* **130**, No. 6, 551–560.

Marquez, R. M. (2004). *Three-dimensional slope stability analysis using finite elements*. Masters thesis, Division of Engineering, Colorado School of Mines.

Matsui, T. & San, K. C. (1992). Finite element slope stability analysis by shear strength reduction technique. *Soils Found.* **32**, No. 1, 59–70.

Perzyna, P. (1966). Fundamental problems in viscoplasticity. *Advances in Applied Mechanics* **9**, 243–377.

Potts, D. M., Dounias, G. T. & Vaughan, P. R. (1990). Finite element analysis of progressive failure of Carsington embankment. *Géotechnique* **40**, No. 1, 79–102.

Sainak, A. N. (2004). Application of three-dimensional finite element method in parametric and geometric studies of slope stability. In *Advances in geotechnical engineering (Skempton Conference)*, Vol. 2, pp. 933–942. London: Thomas Telford.

Seed, R. B., Mitchell, J. K. & Seed, H. B. (1990). Kettleman Hills waste landfill slope failure. II: Stability analysis. *J. Geotech. Engng* **116**, No. 4, 669–689.

Silvestri, V. (2006). A three-dimensional slope stability problem in clay. *Can. Geotech. J.* **43**, No. 2, 224–228.

Smith, I. M. & Griffiths, D. V. (1988). *Programming the finite element method*, 2nd edn. Chichester: John Wiley & Sons.

Smith, I. M. & Griffiths, D. V. (2004). *Programming the finite element method*, 4th edn. Chichester: John Wiley & Sons.

Smith, I. M. & Hobbs, R. (1974). Finite element analysis of centrifuged and built-up slopes. *Géotechnique* **24**, No. 4, 531–559.

Stark, T. D. & Eid, H. T. (1998). Performance of three-dimensional slope stability methods. *J. Geotech. Geoenviron. Engng* **124**, No. 11, 1049–1060.

Xie, M., Esaki, T., Zhou, G. & Mitani, Y. (2003). Geographic information systems-based three-dimensional critical slope stability analysis and landslide hazard assessment. *J. Geotech. Geoenviron. Engng* **129**, No. 12, 1109–1118.

Xie, M. W., Esaki, T. and Cai, M. F. (2006). GIS-based implementation of three-dimensional limit equilibrium approach of slope stability. *J. Geotech. Geoenviron. Engng* **132**, No. 5, 656–660.

Zhang, J. F., Qi, T. & Li, Z. G. (2005a). An extension of 2D Janbu's generalized procedure of slices for 3D slope stability analysis I: Basic theory. *Science in China, Series E-Engineering & Materials Science* **48**, 171–183.

Zhang, J. F., Li, Z. G. & Qi, T. (2005b). An extension of 2D Janbu's generalized procedure of slices for 3D slope stability analysis I: Numerical method and applications. *Science in China, Series E-Engineering & Materials Science* **48**, 184–195.

Zhang, X. (1988). Three-dimensional stability analysis of concave slopes in plan view. *J. Geotech. Engng, ASCE* **114**, No. 6, 658–671.

Zienkiewicz, O. C. (1977). *The finite element method*, 3rd edn. London, New York: McGraw-Hill.

Zienkiewicz, O. C. & Cormeau, I. C. (1974). Viscoplasticity—plasticity and creep in elastic solids: a unified numerical solution approach. *Int. J. Numer. Methods Engng* **8**, No. 4, 821–845.

Zienkiewicz, O. C., Humpheson, C. & Lewis, R. W. (1975). Associated and non-associated viscoplasticity and plasticity in soil mechanics. *Géotechnique* **25**, No. 4, 671–689.